Epitaxial Growth of Flat Antimonene Monolayer: A New Honeycomb Analogue of Graphene

Yan Shao,[†] Zhong-Liu Liu,[†] Cai Cheng,[†] Xu Wu,[†] Hang Liu,[†] Chen Liu,[‡] Jia-Ou Wang,[‡] Shi-Yu Zhu,[†] Yu-Qi Wang,[†] Dong-Xia Shi,[†] Kurash Ibrahim,[‡] Jia-Tao Sun,*[,†] Ye-Liang Wang,*[,†,§] and Hong-Jun Gao[†,§]

[†]Institute of Physics and University of Chinese Academy of Sciences, Chinese Academy of Sciences, Beijing 100190, China
[‡]Institute of High-Energy Physics, Chinese Academy of Sciences, Beijing 100049, China
[§]CAS Center for Excellence in Topological Quantum Computation, Beijing 100049, China

S *Supporting Information*
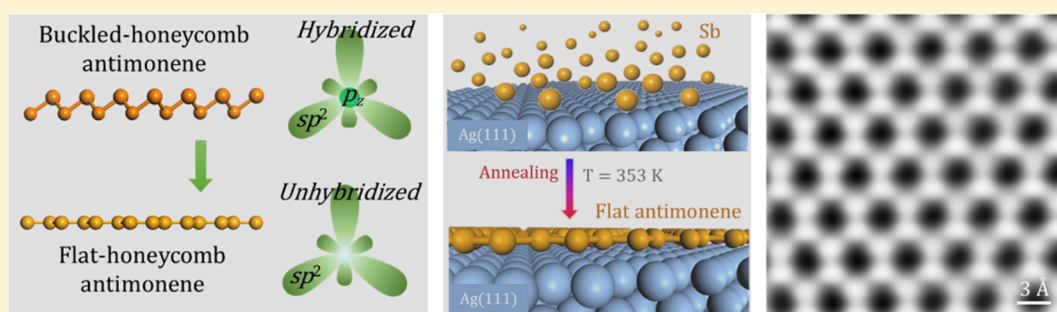
ABSTRACT: Group-V elemental monolayers were recently predicted to exhibit exotic physical properties such as nontrivial topological properties, or a quantum anomalous Hall effect, which would make them very suitable for applications in next-generation electronic devices. The free-standing group-V monolayer materials usually have a buckled honeycomb form, in contrast with the flat graphene monolayer. Here, we report epitaxial growth of atomically thin flat honeycomb monolayer of group-V element antimony on a Ag(111) substrate. Combined study of experiments and theoretical calculations verify the formation of a uniform and single-crystalline antimonene monolayer without atomic wrinkles, as a new honeycomb analogue of graphene monolayer. Directional bonding between adjacent Sb atoms and weak antimonene-substrate interaction are confirmed. The realization and investigation of flat antimonene honeycombs extends the scope of two-dimensional atomically-thick structures and provides a promising way to tune topological properties for future technological applications.

KEYWORDS: *Antimonene, two-dimensional materials, flat honeycomb lattice, epitaxial growth, STM*

T he discovery of graphene with its unique properties and tremendous potential applications spurred the investigation of other monoelemental two-dimensional (2D) materials.[1−8] Specifically, Group-V elemental 2D materials have attracted intensive interest due to their many interesting properties such as tunable band gap, high carrier mobility, topological nontrivial states, and great potential for future applications.[9−17] Group-V 2D materials include black and blue phosphorene, arsenene, antimonene, bismuthene, etc. Among these, antimonene has attracted increasing attention in recent years because it was calculated to have a significant fundamental band gap (2.28 eV)[18] and other excellent properties,[19−29] which make it very suitable for next-generation nanoelectronic devices. In experiments, although the fabrication of antimonene films with different thickness has been realized by different methods,[30−36] the fabrication of high-quality, monolayer antimonene with finite atomic undulations remained to be explored extensively, which may give wider knowledge of the tunable structures and novel properties in a group of elemental materials.

Group-V elements have five valence electrons in the outmost shell of the electron configuration. The buckled honeycomb group-V elemental monolayer, as shown in Figure 1a, involves hybridized orbitals between in-plane sp^2 and out-of-plane p_z bands holding partially hybridized sp^3 bands;[37] see Figure S1 for a detailed discussion of the orbital hybridization. If the group-V elemental monolayer is highly dilated, the buckled monolayer can become a flat honeycomb configuration, as denoted by a flat antimonene monolayer (FAM) in Figure 1b. Unlike the bonding properties of the former buckled structure, in-plane sp^2 orbitals of the Sb atoms in the flat honeycombs do not couple with the out-of-plane p_z orbital, which preserves the in-plane sp^2 orbitals in FAM, similar to the bonding configuration in
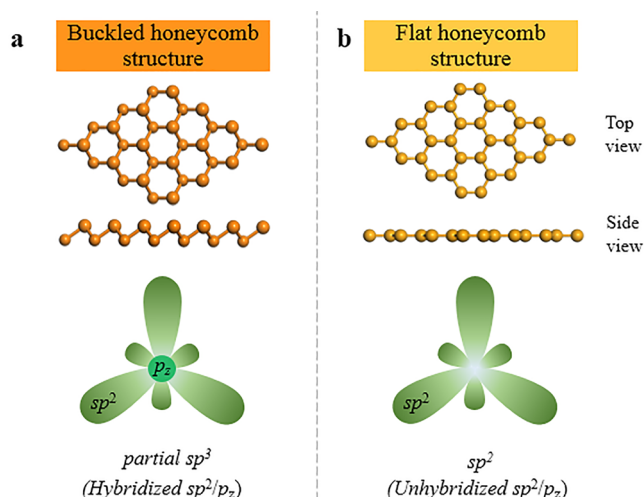
Figure 1. Atomic structures and hybridized orbitals of the buckled and flat honeycombs of antimony: (a) the buckled honeycomb configuration with hybridized orbitals between in-plane sp^2 and out-of-plane p_z (partial sp³) and (b) the flat honeycomb structure with decoupled orbitals between in-plane sp^2 and out-of-plane p_z.

graphene monolayer. The existence of flat antimonene monolayer probably induces unique properties unlike those of its buckled configuration. Indeed, the flat bismuthene monolayer on a SiC substrate has very recently been shown as a promising high-temperature quantum spin Hall material.[38] Being in the same group-V, however, the monolayer antimonene with a flat honeycomb structure, which promises novel electronic properties, has not been experimentally investigated yet.

Here, we report the growth of flat antimonene monolayer (FAM) on a Ag(111) substrate by molecular beam epitaxy

(MBE). Ag(111) is a commonly adopted substrate with hexagonal symmetry and on which it is easy to obtain a clean and defect-free surface, which makes it a good template for the synthesis of 2D honeycomb-like materials such as silicene,[39,40] h-BN,[41] and borophene.[42] In particular, the lattice match between the FAM lattice and the Ag substrate can facilitate the formation of the flat antimony honeycomb lattice on Ag(111). By combining characterization by low-energy electron diffraction (LEED), scanning tunneling microscopy (STM), first-principles calculations and high-resolution STM simulations, we verified the 2D continuous growth of FAM film on the Ag(111) substrate with a unbuckled antimony lattice. The FAM, which inhibits hybridization between in-plane and out-of-plane orbitals, is endowed with the quantum spin Hall effect, showing topologically nontrivial states. This high-quality epitaxial FAM is promising for applications in novel spin-electronic devices, broadening the application field of antimonene.

Figure 2 shows the monolayer antimonene film fabricated by epitaxial growth of antimony atoms on Ag(111) surface. The fabrication process is shown schematically in Figure 2a. The Ag(111) substrate was first cleaned by several cycles of sputtering and annealing until it yielded a distinct Ag (1 × 1) diffraction spot in a LEED pattern (as shown in Figure 2b, circled by a white dashed line) and clean surface terraces in STM images. Then, the antimony (Sb) atoms were deposited onto the as-cleaned Ag(111) substrate kept at 353 K, forming a high-quality monolayer antimony film on it. A total of six new hexagonal diffraction spots, circled by orange dashed line in Figure 2c, are visible and show a $\sqrt{3} \times \sqrt{3}$ superstructure with respect to the Ag(111) surface lattice. The clear and simple LEED pattern in reciprocal space demonstrates the high quality and single crystallinity of the as-grown monolayer antimony film. Furthermore, identical LEED patterns were observed
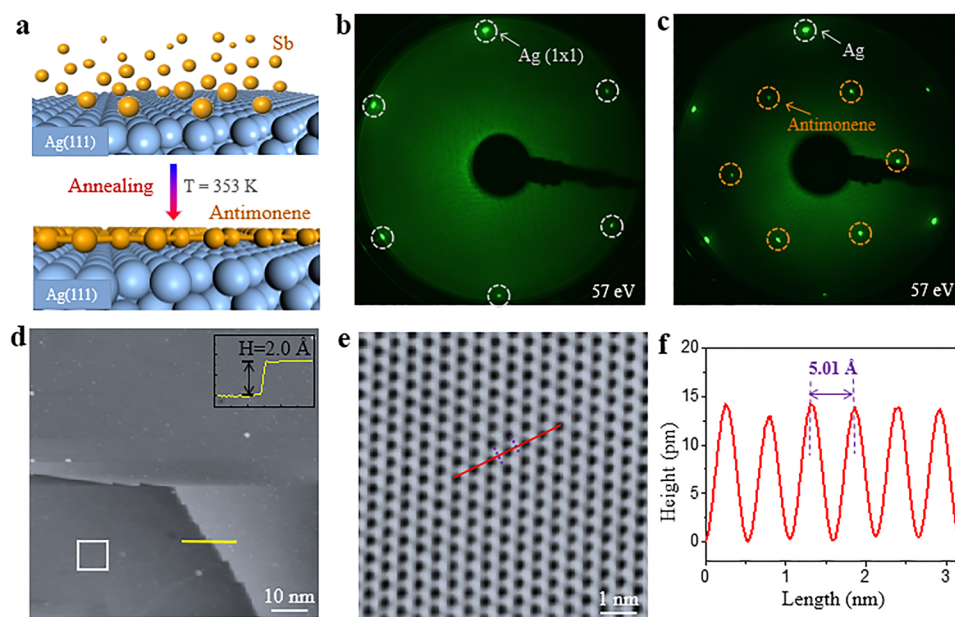
Figure 2. (a) Schematic of fabrication process. (b) LEED pattern of a clean Ag(111) substrate, presenting sharp (1 × 1) diffraction spots. (c) LEED pattern of antimonene on Ag(111), presenting a Ag(111)-($\sqrt{3} \times \sqrt{3}$) superstructure. (d) Large scale STM image of monolayer antimonene on the Ag(111). Inset: A height profile along the yellow line at the terrace edge. The height corresponds to the intrinsic height of Ag(111) terrace, suggesting the Ag(111) terraces are covered fully by monolayer antimonene. (e) High-resolution STM image of antimonene depicted by the white square in panel d, demonstrating a well-ordered honeycomb-like lattice. (f) Line profile corresponding to the red line in panel e, revealing the periodicity of the antimonene lattice (5.01 Å).
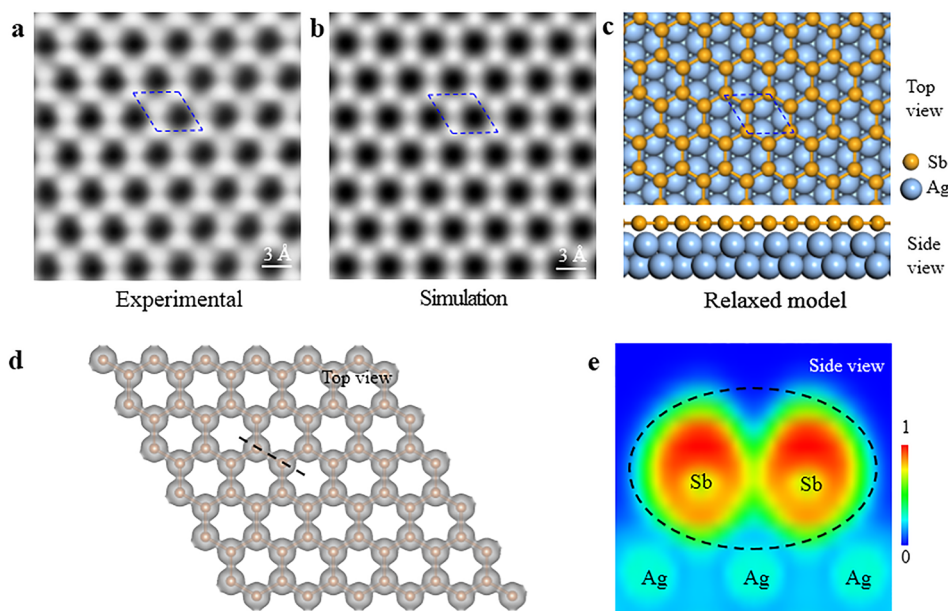
Figure 3. (a) Atomic-resolution STM image of monolayer antimonene on Ag(111). The unit cell of the Ag(111)-($\sqrt{3} \times \sqrt{3}$) superstructure is marked by the blue dashed line. (b) STM simulation of flat monolayer antimonene on Ag(111). (c) Energetically favorable atomic model of monolayer antimonene on Ag(111), showing a honeycomb lattice. Orange (blue) balls represent Sb (Ag) atoms. (d) Top view of the overall electron localization function (ELF) of the relaxed model of FAM, showing the continuity of the monolayer antimonene. (e) Cross-sectional ELF along the black dashed line in panel d, demonstrating high localization of the electrons in Sb−Sb pairs and weak Sb−Ag interaction.

across the entire sample surface (8 mm × 8 mm in size), indicating the growth of a homogeneous and high-quality thin film of monolayer antimony.

To further investigate the structural features of monolayer antimony in real space, STM measurements were carried out. Figure 2d is a typical large scale STM image of the same sample, demonstrating a homogeneous thin film on the entire Ag(111) surface. The apparent height of the antimonene film is 2.2 Å, as measured by decreasing coverage (Figure S2), and in which small submonolayer antimony islands are visible. Here the apparent height is lower than the previously reported buckled monolayer antimonene (2.8 Å),[32,36] suggesting that a single-layer antimonene with a lower buckling configuration has been fabricated on the Ag(111) surface.

Figure 2e shows a zoomed-in STM image of the area designated by the white square in Figure 2d, revealing a well-ordered honeycomb-like lattice. The period of this honeycomb-like lattice, measured along the red profile line, is 5.01 Å, as shown in Figure 2f, which is in excellent agreement with the Ag(111)-($\sqrt{3} \times \sqrt{3}$) superstructure observed in the LEED patterns (The $\sqrt{3}$ times of the lattice constant 2.89 Å of Ag(111) surface is 5.01 Å.). Compared to the lattice constant (4.13 Å) of freestanding antimonene with a buckling configuration,[18] the larger lattice constant of 5.01 Å here indicates that the as-grown antimonene film certainly has a lower buckling configuration on the Ag(111).

Figure 3a shows an atomically resolved STM image of monolayer antimonene film, which clearly reveals a flat graphene-like honeycomb lattice without obvious atomic buckling. In this image, the unit cell of the flat honeycomb lattice is denoted by the blue dashed lines. Each bright protrusion in the unit cell denotes an individual antimony atom. The brightness of these protrusions is almost the same, indicating there is no clear corrugation between two nearest antimony atoms in the monolayer antimonene.

To deeply elucidate the experimental results above, we carried out first-principles calculations by using the Vienna ab initio simulation package (VASP).[43,44] Slab models of monolayer antimony adsorbed on Ag(111) surface were used by considering three adsorption configurations. Their relative locations are denoted by fcc-hollow, hcp-hollow and atop sites of the Ag(111) surface, respectively, taking the center of antimonene hexagon as a reference point (Figure S3). After all three of these models are fully relaxed, the most energetically stable configuration (hcp-hollow sites) are found and shown in Figure 3c. Based on this optimized model, we performed an STM simulation as shown in Figure 3b. It is found that the adjacent antimony atoms have almost the same brightness in the unit cell marked by a dashed-line rhombus in the simulated STM images, which well-reproduced the honeycomb features of the experimental STM image (Figure 3a). Considering together the STM simulations and experimental STM observations, we are safe to conclude that we have successfully fabricated flat antimony honeycomb monolayer on the Ag(111) substrate.

Note that the flat structure of the antimonene monolayer discussed here is due to the alleviation of atomic buckling. This can be clearly seen in that the Sb−Sb bond length (2.89 Å) in the antimonene is as large as that in the bulk form, and this raises the question of whether the Sb−Sb chemical bond remains in this flat configuration. To address this question and further clarify the interaction among Sb atoms, we calculated the electron localization function (ELF), which can be used to evaluate the bonding properties directly from the value of electron localization degree between individual atoms. The value of ELF is in the range limit from 0 to 1, meaning that the localization of electrons ranges from itinerant to localized form. Figure 3d shows the top view of the calculated ELF pattern for the hcp-hollow structure of FAM on Ag(111), demonstrating
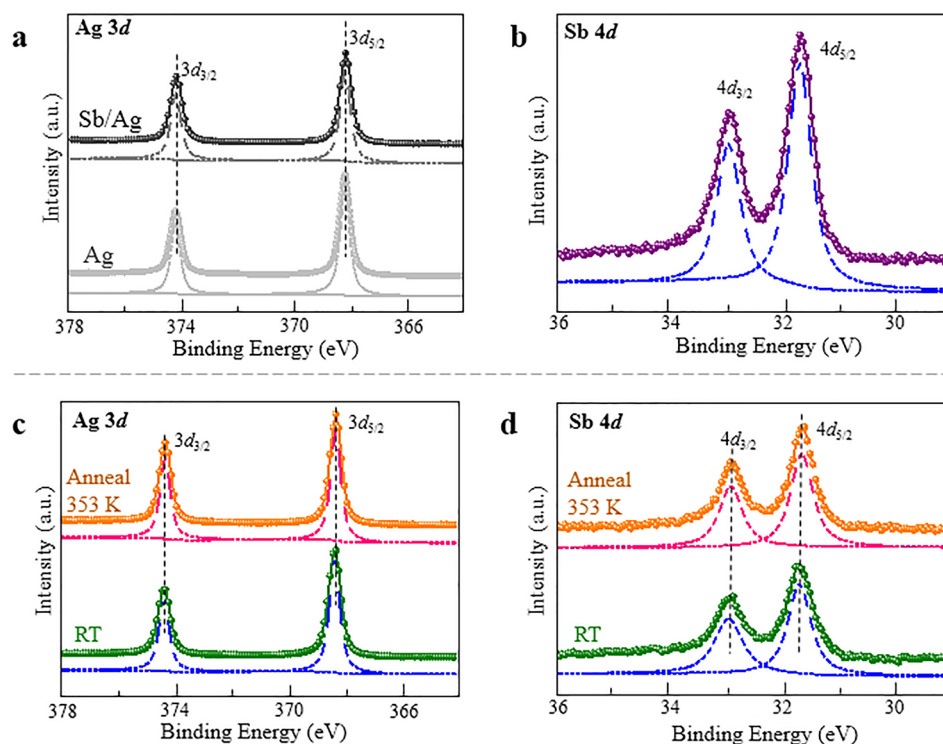
Figure 4. (a) XPS spectra of Ag 3*d* core level before (silver curve) and after (black curve) formation of the antimonene film. The peak positions and shapes undergo almost no changes during formation of the FAM. (b) XPS spectra of Sb 4*d* core level; the two sharp peaks can be assigned to the Sb in antimonene, which demonstrates the formation of the antimonene monolayer. (c, d) The Ag 3*d* and Sb 4*d* core level spectra obtained at room temperature (green curve) and after annealing (orange curve) the sample, in which the positions and shapes of the peaks remain unchanged.

that the electrons of FAM are highly localized around the Sb atoms and the region between adjacent Sb atoms.

To establish the connection between this bonding configuration and its electronic properties, we calculated the band structures of the free-standing FAM. The calculated band structures (Figure S4) show that the FAM is a semi-metal, which is quite different from the semiconducting nature of the buckled antimonene monolayer. This difference signifies the substantial effect of atomic buckling on the electronic structures of elemental monolayers. Moreover, our calculations show that the FAM is a topological semimetal having a topologically nontrivial edge state (depicted by the red line in Figure S4i), significantly different from the properties of the highly buckled configuration (Figure S4c).[20] Furthermore, the out-of-plane p_z orbital of the antimony atoms in the FAM is generally disentangled from the in-plane sp^2 orbitals (Figure S1). The preservation of the out-of-plane p_z orbital forms a gapped Dirac cone (with a gap of 47.7 meV) below the Fermi level (depicted by the shaded circle in Figure S1j), which is similar to the π bonding of graphene. Very recently, this kind of induced topological property was revealed in a flat bismuthene monolayer and shown to contribute to quantum spin Hall effect.[38] Thus, our work may provide an effective and promising way to tune the topological properties of antimonene and broaden related applications.

To further clarify the possible interaction between FAM lattice and the Ag(111) substrate, a cross-sectional ELF pattern perpendicular to the plane of the monolayer antimonene and along the Sb−Sb bonding direction (depicted with the black dashed line in Figure 3d) was calculated and is shown in Figure 3e. It is obvious that electrons are highly localized at the Sb−Sb pair, analogous to carbon atoms in graphene. This provides

direct evidence of a strong chemical interaction between each Sb−Sb pair, responsible for the existence and stability of the structure of antimonene. Moreover, the ELF value between the neighboring Sb atom and the nearest substrate Ag atom is much less than that of the Sb−Sb pair, indicating fairly weak interaction between flat monolayer antimony and the substrate.

To further evaluate the interaction experimentally between the monolayer antimonene and the substrate, X-ray photoelectron spectroscopy (XPS) measurements were carried out to monitor the chemical shift of Ag and Sb elements during the fabrication process. Figure 4a shows the characteristic XPS spectra from the core level of the Ag element before and after the formation of antimonene films (illustrated by silver and black curves, respectively). Before the antimony deposition, the characteristic signals of Ag 3$d_{3/2}$ and 3$d_{5/2}$ appear at the binding energies of 374.18 and 368.18 eV, respectively. After antimonene growth, there is almost no change in the shape and binding energies of these characteristic peaks besides an energy shift of 0.13 eV. This tiny energy shift is probably due to the measurement fluctuation considering the energy resolution of our XPS measurements is about 0.3 eV. There would be an obvious chemical shift in these characteristic peaks if its chemical state of Ag element has changed. For example, silicene grown on the Ag(111) surface caused a ∼0.7 eV chemical shift for Ag 3d electron because of the formation of Si−Ag bonds.[45] Moreover, the shape of the peaks remains the same and no additional peaks appear. This verifies that no chemical shift occurs in Ag atoms during the antimonene film growth. Figure 4b is the XPS core-level spectrum of Sb 4d from the antimonene films. The two characteristic peaks are located at 33.04 and 31.79 eV, respectively, a small shift compared to the peaks of buckled antimonene on PdTe$_2$ and Sb$_2$Te$_3$

substrates,[32,33] mostly owing to the change of the lattice constant. No additional peaks appear, demonstrating the purity and high quality of the as-grown monolayer antimonene. In addition, our XPS measurements of the sample after oxygen exposure showed that no energy shift of the Sb 4d characteristic peaks, demonstrating the chemical stability of the as-grown monolayer antimonene sample in oxygen atmosphere, a promising property for practical application as reported previously in buckling monolayer or few-layer antimony films.[30,32,34,35]

Additionally, depositing Sb atoms on a Ag(111) substrate at room temperature (without the annealing process) can also result in submonolayer antimony islands, a similar behavior found by previous STM studies.[46,47] The islands present the same structural configuration as the monolayer antimony. This sample with an increasing amount of Sb atoms at room temperature followed by an annealing process was measured (Figure S5), which showed that the area of antimonene islands can be increased by extending the deposition time of Sb atoms, and a uniform and high-quality full-layer antimonene can be achieved by a relatively low annealing temperature (353 K). We also used XPS measurements to monitor the chemical shift of Ag and Sb atoms during the annealing process, as illustrated in Figure 4c,d. The characteristic peaks for both Ag and Sb that remain are the same before (green curves) and after (orange curves) the annealing process, demonstrating the unchanged chemical states for both Ag and Sb atoms. Combining the calculations and experimental results above, we can verify the formation of a monolayer antimonene on the Ag(111) substrate with no obvious chemical interfacial coupling between the antimonene and the Ag(111). Exfoliation of these antimonene films from the substrate is also of great importance for its practical usage in the future. Considering the configuration of FAM is sustained by the substrate, a proper capping layer to the sample should be used for the preservation of the flat structure of antimonene films. A following ultrasonication of the sample would be a feasible method to obtain antimonene flakes, which requires in-depth investigation.

In summary, we successfully fabricated high-quality flat antimonene monolayer on a Ag(111) substrate. LEED and STM measurements combined with first-principles calculations confirm the formation of a uniform and single-crystalline antimonene monolayer film with a flat honeycomb structure. XPS measurements and ELF analysis reveal a weak interaction between the antimonene film and the Ag(111) substrate. The as-grown FAM film without atomic buckling is endowed with nontrivial topological edge states. The experimental realization of flat antimonene monolayer provides a good candidate for future applications in spintronics and related nanodevices.

Methods. *Sample Preparation and STM Experiments.* The flat antimonene monolayer was fabricated on a Ag(111) substrate in an ultrahigh-vacuum (UHV) chamber, with a base pressure of 2×10^{-10} mbar, equipped with standard MBE capabilities. The Ag(111) substrate was cleaned by several cycles of sputtering and annealing until it yielded a distinct Ag-(1 × 1) diffraction spot in a LEED pattern and clean surface terraces in STM images. Antimony atoms (Sigma, 99.999%) evaporated from a Knudsen cell were deposited onto the clean Ag(111) substrate and kept at a related low temperature of 353 K to avoid the formation of a possible alloy phase of Sb and Ag. After growth, the sample was transferred to a chamber with LEED and STM equipment for measurements. All STM measurements were performed at room temperature with a chemically etched W tip.

XPS Measurements. The in situ X-ray photoelectron spectroscopy measurements were performed at the Beijing Synchrotron Radiation Facility (BSRF). The samples were stored in a UHV suitcase for transfer among different experimental stations. The synchrotron radiation monochromated light by 4 high-resolution gratings and controlled by a hemispherical energy analyzer has a photon energy in the range from 10 to 1100 eV in the energy resolution of 0.3 eV. The photon energy of XPS experiments was 500 eV for Ag 3d and 180 eV for Sb 4d measurements, respectively.

Calculation Method. The first-principles calculations within the framework of density functional theory were carried out using the Vienna ab initio simulation package (VASP). The projector augmented-wave method[43] and Perdew−Burke−Ernzerhof exchange-correlation functional[48] were used. A cutoff energy of 400 eV for the plane-wave basis set and a Monkhorst−Pack mesh[49] of 9 × 9 × 1 for the Brillouin zone integration were employed for self-consistent calculations. The interfacial interaction between FAM and Ag(111) substrate were investigated by putting FAM on a 10-layer slab of Ag(111)-($\sqrt{3} \times \sqrt{3}$)R 30° surface in the registry. To eliminate spurious interaction between two adjacent slabs, a vacuum layer of thickness larger than 17 Å is applied. The atomic structures were fully relaxed until the force on each atom was less than 0.01 eV/Å with the bottom four layers of silver atoms fixed. The simulated STM images were obtained by calculating the local density of states in the Tersoff−Hamann approximation.

■ ASSOCIATED CONTENT

Ⓢ Supporting Information

The Supporting Information is available free of charge on the ACS Publications website at DOI: 10.1021/acs.nanolett.8b00429.

> Additional details on the atomic models and projected band structures of the buckled and flat antimonene honeycombs, antimonene islands on Ag(111), first-principles calculations for three different models of monolayer antimonene on Ag(111), the influence of atomic buckling on the band structures and edge states, and the formation of antimonene film with and without the annealing process. (PDF)

■ AUTHOR INFORMATION

Corresponding Authors
*E-mail: jtsun@iphy.ac.cn. Phone: (+86)-10-82649930.
*E-mail: ylwang@iphy.ac.cn. Phone: (+86)-10-82648072.

ORCID Ⓞ
Jia-Tao Sun: 0000-0003-3519-352X
Ye-Liang Wang: 0000-0002-8896-0748
Hong-Jun Gao: 0000-0002-6766-0623

Author Contributions

Y.S. and Z.L.L. contributed equally to this work. The manuscript was written through contributions of all authors.

Notes

The authors declare no competing financial interest.

■ ACKNOWLEDGMENTS

■ REFERENCES

(1) Novoselov, K. S.; Mishchenko, A.; Carvalho, A.; Castro Neto, A. H. 2D Materials and van der Waals Heterostructures. *Science* **2016**, *353* (6298), 9439.

(2) Mannix, A. J.; Kiraly, B.; Hersam, M. C.; Guisinger, N. P. Synthesis and Chemistry of Elemental 2D Materials. *Nat. Rev. Chem.* **2017**, *1* (2), 0014.

(3) Tan, C.; Cao, X.; Wu, X. J.; He, Q.; Yang, J.; Zhang, X.; Chen, J.; Zhao, W.; Han, S.; Nam, G. H.; Sindoro, M.; Zhang, H. Recent Advances in Ultrathin Two-Dimensional Nanomaterials. *Chem. Rev.* **2017**, *117* (9), 6225–6331.

(4) Molle, A.; Goldberger, J.; Houssa, M.; Xu, Y.; Zhang, S. C.; Akinwande, D. Buckled Two-Dimensional Xene Sheets. *Nat. Mater.* **2017**, *16* (2), 163.

(5) Meng, L.; Wang, Y.; Zhang, L.; Du, S.; Wu, R.; Li, L.; Zhang, Y.; Li, G.; Zhou, H.; Hofer, W. A.; Gao, H. J. Buckled Silicene Formation on Ir(111). *Nano Lett.* **2013**, *13* (2), 685–690.

(6) Li, L.; Wang, Y.; Xie, S.; Li, X. B.; Wang, Y. Q.; Wu, R.; Sun, H.; Zhang, S.; Gao, H. J. Two-Dimensional Transition Metal Honeycomb Realized: Hf on Ir(111). *Nano Lett.* **2013**, *13* (10), 4671–4674.

(7) Li, L.; Lu, S. Z.; Pan, J.; Qin, Z.; Wang, Y. Q.; Wang, Y.; Cao, G. Y.; Du, S.; Gao, H. J. Buckled Germanene Formation on Pt(111). *Adv. Mater.* **2014**, *26* (28), 4820–4824.

(8) Huang, L.; Zhang, Y. F.; Zhang, Y. Y.; Xu, W.; Que, Y.; Li, E.; Pan, J. B.; Wang, Y. L.; Liu, Y.; Du, S. X.; Pantelides, S. T.; Gao, H. J. Sequence of Silicon Monolayer Structures Grown on a Ru Surface: from a Herringbone Structure to Silicene. *Nano Lett.* **2017**, *17* (2), 1161–1166.

(9) Zhang, S.; Guo, S.; Chen, Z.; Wang, Y.; Gao, H.; Gomez-Herrero, J.; Ares, P.; Zamora, F.; Zhu, Z.; Zeng, H. Recent Progress in 2D Group-VA Semiconductors: from Theory to Experiment. *Chem. Soc. Rev.* **2018**, *47*, 982.

(10) Pumera, M.; Sofer, Z. 2D Monoelemental Arsenene, Antimonene, and Bismuthene: Beyond Black Phosphorus. *Adv. Mater.* **2017**, *29* (21), 1605299.

(11) Zhang, S.; Xie, M.; Li, F.; Yan, L.; Kan, E.; Liu, W.; Chen, Z.; Zeng, H.; Li, Y. Semiconducting Group 15 Monolayers: A Broad Range of Band Gaps and High Carrier Mobilities. *Angew. Chem.* **2016**, *128*, 1698–1701.

(12) Tran, V.; Soklaski, R.; Liang, Y.; Yang, L. Layer-Controlled Band Gap and Anisotropic Excitons in Few-Layer Black Phosphorus. *Phys. Rev. B: Condens. Matter Mater. Phys.* **2014**, *89* (23), 5319.

(13) Li, L.; Yu, Y.; Ye, G. J.; Ge, Q.; Ou, X.; Wu, H.; Feng, D.; Chen, X. H.; Zhang, Y. Black Phosphorus Field-Effect Transistors. *Nat. Nanotechnol.* **2014**, *9* (5), 372–377.

(14) Qiao, J.; Kong, X.; Hu, Z. X.; Yang, F.; Ji, W. High-Mobility Transport Anisotropy and Linear Dichroism in Few-Layer Black Phosphorus. *Nat. Commun.* **2014**, *5*, 4475–4482.

(15) Zhang, J. L.; Zhao, S.; Han, C.; Wang, Z.; Zhong, S.; Sun, S.; Guo, R.; Zhou, X.; Gu, C. D.; Yuan, K. D.; Li, Z.; Chen, W. Epitaxial Growth of Single Layer Blue Phosphorus: A New Phase of Two-Dimensional Phosphorus. *Nano Lett.* **2016**, *16* (8), 4903–4908.

(16) Sun, J. T.; Huang, H.; Wong, S. L.; Gao, H. J.; Feng, Y. P.; Wee, A. T. Energy-Gap Opening in a Bi(110) Nanoribbon Induced by Edge Reconstruction. *Phys. Rev. Lett.* **2012**, *109* (24), 6804.

(17) Drozdov, I. K.; Alexandradinata, A.; Jeon, S.; Nadj-Perge, S.; Ji, H.; Cava, R. J.; Andrei Bernevig, B.; Yazdani, A. One-Dimensional Topological Edge States of Bismuth Bilayers. *Nat. Phys.* **2014**, *10* (9), 664–669.

(18) Zhang, S.; Yan, Z.; Li, Y.; Chen, Z.; Zeng, H. Atomically Thin Arsenene and Antimonene: Semimetal-Semiconductor and Indirect-Direct Band-Gap Transitions. *Angew. Chem., Int. Ed.* **2015**, *54*, 3112–3115.

(19) Wang, G.; Pandey, R.; Karna, S. P. Atomically Thin Group V Elemental Films: Theoretical Investigations of Antimonene Allotropes. *ACS Appl. Mater. Interfaces* **2015**, *7* (21), 11490–11496.

(20) Chuang, F. C.; Hsu, C. H.; Chen, C. Y.; Huang, Z. Q.; Ozolins, V.; Lin, H.; Bansil, A. Tunable Topological Electronic Structures in Sb(111) Bilayers: a First-Principles Study. *Appl. Phys. Lett.* **2013**, *102* (2), 022424.

(21) Wang, Y.; Huang, P.; Ye, M.; Quhe, R.; Pan, Y.; Zhang, H.; Zhong, H.; Shi, J.; Lu, J. Many-body Effect, Carrier Mobility, and Device Performance of Hexagonal Arsenene and Antimonene. *Chem. Mater.* **2017**, *29* (5), 2191–2201.

(22) Gupta, S. K.; Sonvane, Y.; Wang, G.; Pandey, R. Size and Edge Roughness Effects on Thermal Conductivity of Pristine Antimonene Allotropes. *Chem. Phys. Lett.* **2015**, *641*, 169–172.

(23) Singh, D.; Gupta, S. K.; Sonvane, Y.; Lukačević, I. Antimonene: a Monolayer Material for Ultraviolet Optical Nanodevices. *J. Mater. Chem. C* **2016**, *4* (26), 6386–6390.

(24) Zhang, S.; Zhou, W.; Ma, Y.; Ji, J.; Cai, B.; Yang, S. A.; Zhu, Z.; Chen, Z.; Zeng, H. Antimonene Oxides: Emerging Tunable Direct Bandgap Semiconductor and Novel Topological Insulator. *Nano Lett.* **2017**, *17* (6), 3434–3440.

(25) Pizzi, G.; Gibertini, M.; Dib, E.; Marzari, N.; Iannaccone, G.; Fiori, G. Performance of Arsenene and Antimonene Double-Gate MOSFETS from First Principles. *Nat. Commun.* **2016**, *7*, 12585.

(26) Wang, S.; Wang, W.; Zhao, G. Thermal Transport Properties of Antimonene: an Ab Initio Study. *Phys. Chem. Chem. Phys.* **2016**, *18* (45), 31217–31222.

(27) Zhang, P.; Liu, Z.; Duan, W.; Liu, F.; Wu, J. Topological and Electronic Transitions in a Sb(111) Nanofilm: the Interplay Between Quantum Confinement and Surface Effect. *Phys. Rev. B: Condens. Matter Mater. Phys.* **2012**, *85* (20), 1410.

(28) Bian, G.; Miller, T.; Chiang, T. C. Passage from Spin-Polarized Surface States to Unpolarized Quantum Well States in Topologically Nontrivial Sb Films. *Phys. Rev. Lett.* **2011**, *107* (3), 6802.

(29) Bian, G.; Wang, X.; Liu, Y.; Miller, T.; Chiang, T. C. Interfacial Protection of Topological Surface States in Ultrathin Sb Films. *Phys. Rev. Lett.* **2012**, *108* (17), 6401.

(30) Ares, P.; Aguilar-Galindo, F.; Rodriguez-San-Miguel, D.; Aldave, D. A.; Diaz-Tendero, S.; Alcami, M.; Martin, F.; Gomez-Herrero, J.; Zamora, F. Mechanical Isolation of Highly Stable Antimonene Under Ambient Conditions. *Adv. Mater.* **2016**, *28* (30), 6332–6336.

(31) Gibaja, C.; Rodriguez-San-Miguel, D.; Ares, P.; Gomez-Herrero, J.; Varela, M.; Gillen, R.; Maultzsch, J.; Hauke, F.; Hirsch, A.; Abellan, G.; Zamora, F. Few-Layer Antimonene by Liquid-Phase Exfoliation. *Angew. Chem., Int. Ed.* **2016**, *55*, 14345–14349.

(32) Wu, X.; Shao, Y.; Liu, H.; Feng, Z.; Wang, Y. L.; Sun, J. T.; Liu, C.; Wang, J. O.; Liu, Z. L.; Zhu, S. Y.; Wang, Y. Q.; Du, S. X.; Shi, Y. G.; Ibrahim, K.; Gao, H. J. Epitaxial Growth and Air-Stability of Monolayer Antimonene on PdTe$_2$. *Adv. Mater.* **2017**, *29*, 1605407.

(33) Lei, T.; Liu, C.; Zhao, J.-L.; Li, J.-M.; Li, Y.-P.; Wang, J.-O.; Wu, R.; Qian, H.-J.; Wang, H.-Q.; Ibrahim, K. Electronic Structure of Antimonene Grown on Sb$_2$Te$_3$ (111) and Bi$_2$Te$_3$ Substrates. *J. Appl. Phys.* **2016**, *119* (1), 015302.

(34) Fortin-Deschenes, M.; Waller, O.; Mentes, T. O.; Locatelli, A.; Mukherjee, S.; Genuzio, F.; Levesque, P. L.; Hebert, A.; Martel, R.; Moutanabbir, O. Synthesis of Antimonene on Germanium. *Nano Lett.* **2017**, *17* (8), 4970–4975.

(35) Ji, J.; Song, X.; Liu, J.; Yan, Z.; Huo, C.; Zhang, S.; Su, M.; Liao, L.; Wang, W.; Ni, Z.; Hao, Y.; Zeng, H. Two-Dimensional Antimonene Single Crystals Grown by van der Waals Epitaxy. *Nat. Commun.* **2016**, *7*, 13352.

(36) Kim, S. H.; Jin, K. H.; Park, J.; Kim, J. S.; Jhi, S. H.; Yeom, H. W. Topological Phase Transition and Quantum Spin Hall Edge States of Antimony Few Layers. *Sci. Rep.* **2016**, *6*, 33193.

(37) Castro Neto, A. H.; Guinea, F. Impurity-Induced Spin-Orbit Coupling in Graphene. *Phys. Rev. Lett.* **2009**, *103* (2), 6804.

(38) Reis, F.; Li, G.; Dudy, L.; Bauernfeind, M.; Glass, S.; Hanke, W.; Thomale, R.; Schafer, J.; Claessen, R. Bismuthene on a SiC Substrate:

a Candidate for a High-Temperature Quantum Spin Hall Material. *Science* **2017**, *357* (6348), 287−290.

(39) Feng, B.; Ding, Z.; Meng, S.; Yao, Y.; He, X.; Cheng, P.; Chen, L.; Wu, K. Evidence of Silicene in Honeycomb Structures of Silicon on Ag(111). *Nano Lett.* **2012**, *12* (7), 3507−3511.

(40) Vogt, P.; De Padova, P.; Quaresima, C.; Avila, J.; Frantzeskakis, E.; Asensio, M. C.; Resta, A.; Ealet, B.; Le Lay, G. Silicene: Compelling Experimental Evidence for Graphenelike Two-Dimensional Silicon. *Phys. Rev. Lett.* **2012**, *108* (15), 5501.

(41) Müller, F.; Hüfner, S.; Sachdev, H.; Laskowski, R.; Blaha, P.; Schwarz, K. Epitaxial Growth of Hexagonal Boron Nitride on Ag(111). *Phys. Rev. B: Condens. Matter Mater. Phys.* **2010**, *82* (11), 3406.

(42) Feng, B.; Zhang, J.; Zhong, Q.; Li, W.; Li, S.; Li, H.; Cheng, P.; Meng, S.; Chen, L.; Wu, K. Experimental Realization of Two-Dimensional Boron Sheets. *Nat. Chem.* **2016**, *8* (6), 563−568.

(43) Blöchl, P. E. Projector Augmented-Wave Method. *Phys. Rev. B: Condens. Matter Mater. Phys.* **1994**, *50* (24), 17953−17979.

(44) Kresse, G.; Furthmüller, J. Efficient Iterative Schemes for Ab Initio Total-Energy Calculations Using a Plane-Wave Basis Set. *Phys. Rev. B: Condens. Matter Mater. Phys.* **1996**, *54* (16), 11169−11186.

(45) Xu, X.; Zhuang, J.; Du, Y.; Feng, H.; Zhang, N.; Liu, C.; Lei, T.; Wang, J.; Spencer, M.; Morishita, T.; Wang, X.; Dou, S. X. Effects of Oxygen Adsorption on the Surface State of Epitaxial Silicene on Ag(111). *Sci. Rep.* **2014**, *4*, 7543.

(46) van der Vegt, H. A.; Vrijmoeth, J.; Behm, R. J.; Vlieg, E. Sb-Enhanced Nucleation in the Homoepitaxial Growth of Ag(111). *Phys. Rev. B: Condens. Matter Mater. Phys.* **1998**, *57* (7), 4127−4131.

(47) Meyer, J. A.; van der Vegt, H. A.; Vrijmoeth, J.; Vlieg, E.; Behm, R. J. Reversible Place-Exchange during Film Growth: a Mechanism for Surfactant Transport. *Surf. Sci.* **1996**, *355* (1−3), 375−380.

(48) Perdew, J. P.; Burke, K.; Ernzerhof, M. Generalized Gradient Approximation Made Simple. *Phys. Rev. Lett.* **1996**, *77* (18), 3865−3868.

(49) Monkhorst, H. J.; Pack, J. D. Special Points for Brillouin-Zone Integrations. *Phys. Rev. B: Condens. Matter Mater. Phys.* **1976**, *13* (12), 5188−5192.